Hindawi Publishing Corporation
Journal of Sensors
Volume 2012, Article ID 961239, 8 pages
doi:10.1155/2012/961239

Research Article

Modelling of Atomic Imaging and Evaporation in the Field Ion Microscope

Keith J. Fraser and John J. Boland

School of Chemistry and CRANN, Trinity College Dublin, Dublin 2, Ireland

Correspondence should be addressed to Keith J. Fraser, fraserk@tcd.ie

Received 15 June 2011; Revised 17 September 2011; Accepted 18 September 2011

Academic Editor: Sangmin Jeon

Imaging and evaporation of atoms in the field ion microscope (FIM) has been modelled by using finite difference methods to calculate the voltage distribution around a tip and hence the electric field strength experienced by individual atoms. Atoms are evaporated based on field strength using a number of different mathematical models which yield broadly similar results. The tip shapes and simulated FIM images produced show strong agreement with experimental results for tips of the same orientation and crystal structure. Calculations have also been made to estimate the effects on resolution of using a field-sharpened tip for scanning probe microscopy.

1. Introduction

Field ion microscopy (FIM) has been used by several groups to examine and prepare tungsten tips for scanning tunnelling microscopy (STM) and atomic force microscopy (AFM) [1–3]. Field evaporation can produce a tip apex consisting of only a few atoms or even a single atom. The imaging resolution is reported to be improved through the use of tips sharpened in this way; however, this has generally not been quantified or investigated systematically. The forces measured in AFM operate over longer ranges than the tunnelling current measured in STM and are thus more sensitive to the atomic structure of the tip beyond the apex. Our aim is to numerically model field-induced tip sharpening in order to better understand the phenomenon and quantify the tip shapes produced, with a view to refining/designing scanning probe microscope (SPM) tip sharpening procedures and choosing the optimal materials.

Various theoretical studies have been carried out in the past on evaporation of atoms from tips under high electric fields; most of these have been aimed at simulating imaging in the 3D atom probe (e.g., the work of Geiser, Marquis et al. [4, 5]) and have therefore focused on the trajectories of evaporated ions rather than on the evolution of the atomic structure of the tip and its application to scanning probe microscopy. Our work builds on aspects of the approach of Vurpillot et al. [6], exploring alternative methods for determining which atoms undergo field evaporation and extending to different tip materials and orientations. *W* tips oriented along the 110 and 111 directions and Pt tips oriented in the 100 direction are discussed here. *W* tips are most commonly used in SPM, with the 110 orientation being observed in FIM experiments on tips made from polycrystalline wire and 111-oriented tips made from single-crystal wire being used in some experiments. Pt tips were considered due to future plans to use noble-metal-coated Si cantilever tips for combined AFM/STM.

2. Method

2.1. Overview. Here we introduce a modelling program capable of generating and simulating tips of different geometric shapes (including faceted tips) or materials and with different values of the aspect ratio between length and base radius. The tip surface and surrounding vacuum are modelled as a series of cells of fixed size—in contrast to the studies discussed above where the focus was on image formation, it was not necessary for this model to operate over large differences in length scale, so a variable mesh was not used.

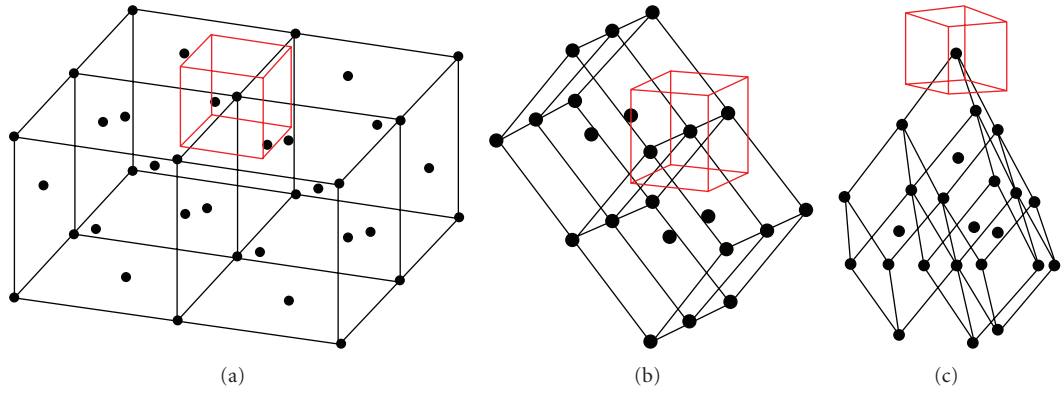

Figure 1: Illustration of cell shapes used for different crystal structures and orientations, compared with crystal unit cells: (a) face-centred cubic (100 orientation), (b) body-centred cubic (110 orientation), and (c) body-centred cubic (111 orientation). Atoms and unit cells shown in black; model cells shown in red.

Each cell is centred on an atomic site as shown in Figure 1. The cell shape and dimensions are dictated by the tip's crystal structure and orientation; the cell z-axis is oriented along the tip axis with the x- and y-axes defined by the shortest interatomic distances in the plane perpendicular to the tip axis. In simple cubic materials, each cubical cell (Figure 1(a)) contains one atom; in other crystal systems, some cells are empty due to the periodicity and the cell shape is different. In the 110 orientation, the cell is a cuboid (Figure 1(b)), while in the 110 orientation it is a prism where the base is a rhombus with an interior angle of 120°.

The voltage distribution around the tip is calculated using a finite difference approximation in which the voltage within each cell is held constant. Within the tip surface, the voltage is set equal to the applied voltage V_0. Far from the tip, the voltage is set to zero. The voltage in the remaining cells is calculated using these boundary conditions and Poisson's equation ($\nabla^2 V = 0$). The resulting series of simultaneous equations is solved iteratively for the values of voltage in each cell. Steady state is deemed to have been reached when the deviation from Poisson's equation summed over all cells falls below a set threshold.

The electric field experienced by each atom at the tip surface is equal to the gradient of the voltage distribution ($F = \nabla V$) and is calculated under the finite difference approximation using the difference between voltage values in adjacent cells and the cell dimensions. When an atom chosen according to the criteria discussed below is evaporated from the tip surface, the voltage distribution is recalculated to steady state in all the cells, including those now outside the tip surface. This simulates the change in potential distribution caused by the removal of the evaporated atom.

The values of electric field calculated at each surface atomic site are also used to simulate a field ion image of the tip for comparison with experiment. Atoms experiencing a field above a set threshold are assumed to appear on a field ion image, which thus consists of a series of bright spots corresponding to these atoms (this does not take into account convolution of the image due to bending of the field lines near the tip). Scaling can be added to the image so that the brightness of individual atoms reflects the extent to which the field they experience exceeds the threshold value (Figure 2). Images obtained in this fashion are only schematic as convolution due to variations in ion trajectory between the tip, and FIM screen is not taken into account.

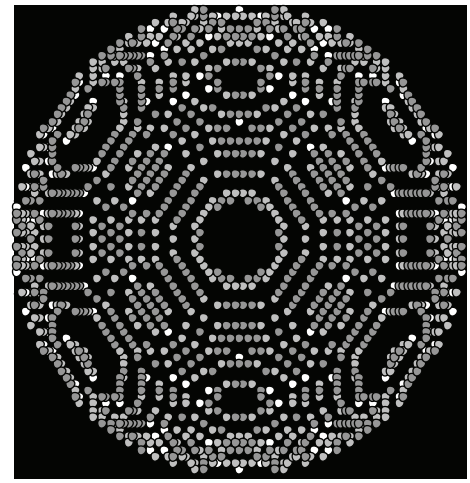

Figure 2: Schematic field ion image of a hemispherical 110-oriented W tip (radius ~8 nm, or 50 atomic spacings in the 100 direction) displaying surface atoms experiencing a field within the indicated bounds (expressed as a function of the maximum field).

To allow larger tips to be modelled in acceptable lengths of time, tip symmetry is used as a means of reducing the number of calculations carried out per iteration when solving for the steady-state voltage distribution. 100- and 110-oriented tips have 4-fold symmetry, while 111-oriented tips have 3-fold symmetry. As a result, only just over 1/4 or 1/3 of the tip need be considered by the model.

Processing speed is also increased by initially treating the tip as radially symmetric and modelling the voltage distribution up to steady-state using cylindrical coordinates. The results are then converted into a three-dimensional coordinate

system and recalculated to steady-state before beginning field evaporation. Only cells within a set distance of the tip surface are converted in this way, reducing the overall number of cells and again increasing the tip size that can be simulated; the voltage outside this region is assumed to remain constant during evaporation. This approximation is found not to significantly affect results provided the cutoff distance is set high enough.

2.2. Field Evaporation Mechanisms. In the simplest form of the model, the surface atom chosen for evaporation is the one which experiences the highest field [6]. This method does not calculate the time between evaporation events or adjustments in the applied voltage; it therefore provides less information about the evaporation process to compare with experimental results. A more sophisticated, time-dependent approach is to calculate the effect of the field on the activation energy for field evaporation. Several mathematical models exist for this [7]; in this work, those used were the image-force model [8] and the approach of Kreuzer and Nath using the universal binding-energy curve [9]. These models use approximations that do not reflect the true nature of the tip surface (e.g., the image-force model is based on the removal of an ion from a flat surface under a field that is constant with distance), but have been found to produce results consistent with experiment for some materials.

Under the image-force model, the activation energy E_A at field F for an n-fold charged ion is given by (1), where Λ is the heat of sublimation of a neutral atom (also known as the cohesive energy), I_n is the nth ionization energy, and Φ_e is the work function. A polarization term $c_a F^2$ can optionally be included [7], where c_a is an empirical coefficient with a value of around 1 meVnm^{2}V^{-2}:

$$E_A = \Lambda + \sum_n I_n - n\Phi_e - \sqrt{\frac{n^3 e^3 F}{4\pi\varepsilon_0}}. \quad (1)$$

The approach of Kreuzer and Nath, shown in (2), expresses the activation energy in terms of the parameter $\delta = F/F_{\text{ev}}$, where F_{ev} is the value of field at which $E_A = 0$. F_{ev} can be calculated for a given material using (3), where λ is the Thomas-Fermi screening length

$$\frac{EA}{\Lambda} = \delta^{1/2} + \frac{1}{2}(1-\delta)\,\text{In}\left(\frac{1-\delta^{1/2}}{1-\delta^{1/2}}\right), \quad (2)$$

$$F_{\text{ev}} = \frac{3\Lambda}{2ne\lambda}. \quad (3)$$

When the activation energy for field evaporation is calculated using (1) or (2), the probability of evaporation for a given atom in the interval between time t and time $t+\tau_0$, where τ_0 is the inverse of the atomic vibration frequency, is given by the expression $p = \exp(-E_A/kT)$, based on the evaporation rate formula $R = (1/\tau_0)\exp(-E_A/kT)$ [8]. To take into account changes in local field as the voltage is ramped and/or atoms evaporate, a cumulative probability is recorded as time passes for each surface atom. Once this probability reaches 1, the atom is evaporated and the cumulative value reset to zero for the newly revealed atom below.

At present, it is assumed that the energy barrier for field evaporation is the same for all atoms. In real materials, the zero-field evaporation energy will vary. Calculating the binding energy for every atom on the tip surface would be highly complex for a tip of significant size; differences in binding energy may be approximated with a simple weighting function that adjusts the value depending on the number of adjacent atoms. A similar approach was used by Vurpillot et al. [6] to simulate evaporation from a tip made up of more than one element.

The different mechanisms are found to produce similar but not identical results. The applied voltage at which evaporation begins to occur varies between the three time-dependent methods; the polarization term in the image-force model increases this threshold by ~20% in the case of $W(110)$ tips, whereas the value under the Kreuzer-Nath model depends on the set value of evaporation field. The single-atom tip (SAT) produced for a tip of a given starting size and shape looks almost exactly the same regardless of which criteria are used (Figures 3(a)–3(d)). The principal difference between the methods is the stability of the single-atom tip. The image-force model and to a lesser extent the Kreuzer-Nath model predict the SAT to persist for a relatively high number of evaporation events before the apex atom is lost, whereas evaporation at highest field predicts that the single-atom tip will be lost almost immediately after forming.

Figures 3(e)–3(h) show the formation of a SAT produced on a polycrystalline W sample which persisted for ~30 s before the voltage was turned down. The dot at the centre of the tip apex in Figures 3(g)–3(h) is assumed to be a single atom rather than a cluster as the same structure was seen in separate experiments and for successive evaporations of layers of material, with the dot disappearing in a single evaporation event. Atoms were observed to evaporate from below the apex during this period, as predicted by the time-dependent models, suggesting that as expected, these models better simulate real field evaporation behaviour. All the results presented in the rest of this paper use the image-force method without polarization.

2.3. Simulating Effect of Tip Sharpening on SPM Resolution. Since the purpose of this work is to investigate the production of sharpened SPM tips using field evaporation, a method is required to quantify the expected effect of a given tip shape on SPM resolution. This is accomplished by calculating the variation of the interatomic force or tunnelling current as the tip is scanned over a feature on a flat surface and using the results to create a schematic AFM or STM image. The signal can be plotted directly to simulate scanning in constant-height mode, or the scan height can be adjusted as a function of position to create a topographical image.

The force between the tip and sample is calculated using the 8-6 Lennard-Jones potential (4), where the negative term represents the attractive van der Waals force, while the positive term is an empirical representation of the electrostatic repulsion. The 8-6 potential was used in preference to the 12-6 potential as it is less computationally expensive and is considered more suitable for nonbonding interactions [10].

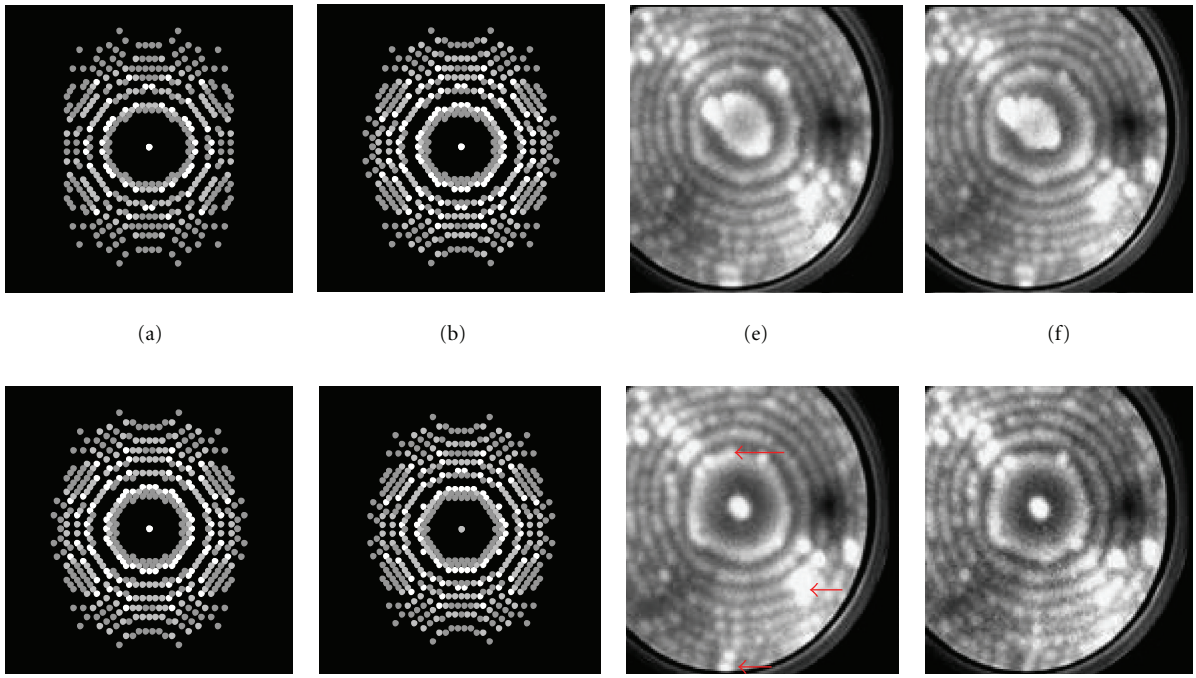

FIGURE 3: (a–d) Schematic field ion images of single-atom $W(110)$ tips produced from a hemispherical starting tip (radius 8 nm) via field evaporation according to highest-field, image-force (with/without polarization), and Kreuzer-Nath criteria; (e–h) experimental field ion images (voltage ~8.8 kV) showing the formation of an SAT and evaporation of atoms from below the apex. Arrows indicate features which change between (g) and (h).

The quantity r is the distance between the atomic centres, and r_m is a factor denoting the distance at which the energy reaches a minimum, set to 3 Å in all the calculations used here. The vertical force acting between the two atoms is given by $-\delta E/\delta z$. The resulting force between each atom in the tip and each atom in the imaged feature is calculated and added to the total force. The surface below is considered to have uniform atomic density, and the force is integrated over and through it in all directions to calculate the "background" signal for each tip atom which is added to the total force. The remainder of the tip shank above the portion of the tip modelled on the atomic scale is also factored in the longer-ranged attractive force which is integrated over a uniform truncated cone and over and through the surface,

$$E \propto \frac{3}{4}\frac{r_m^2}{r^8} - \frac{1}{r^6}. \tag{4}$$

The tunnelling current across a gap s is given by (5), where $\kappa = [m_e(V-E)e]^{0.5}/\hbar$; m_e is the electron mass and $V - E$ (taken as 4 eV) is the tunnelling barrier height. For the purposes of calculating tunnelling current, the tip and sample atoms are considered to be spheres with radii based on the interatomic distance in the crystal lattice, and s is the edge-to-edge distance between two atoms (i.e., the centre-to-centre distance minus the sum of their radii). To calculate the total current, (5) is used to calculate the current through each imaged atom and integrated over the sample surface for each atom on the tip surface,

$$I \propto \exp(-2\kappa s). \tag{5}$$

The results are shown in Figure 4 for the imaging of a single-raised atom on a flat surface by two $W(110)$ tips of similar size, one hemispherical with a flat apex and the other an idealized cone with a single-atom apex. The setpoint in AFM mode is defined as the point of maximum attractive force (i.e., the point where the total force is a minimum). This was chosen as the simplest method of maintaining a short-tip-sample separation. The setpoint current in STM mode was the same for both tips. In both modes, the conical tip gives vastly superior lateral resolution and increased vertical displacement. The latter indicates that the imaged atom produces a greater perturbation in the force or tunnelling current signal relative to the background signal from the underlying surface, which will lead to improved experimental signal-to-noise ratios. The hemispherical tip produces an image of the atomic corrugation of its apex rather than of the sample atom (image convolution) due to each apex atom interacting with the sample atom as they pass over it. The perturbation to the total signal due to the sample atom, and thus the vertical displacement, is smaller due to the larger number of atoms in the blunt tip producing a larger background signal.

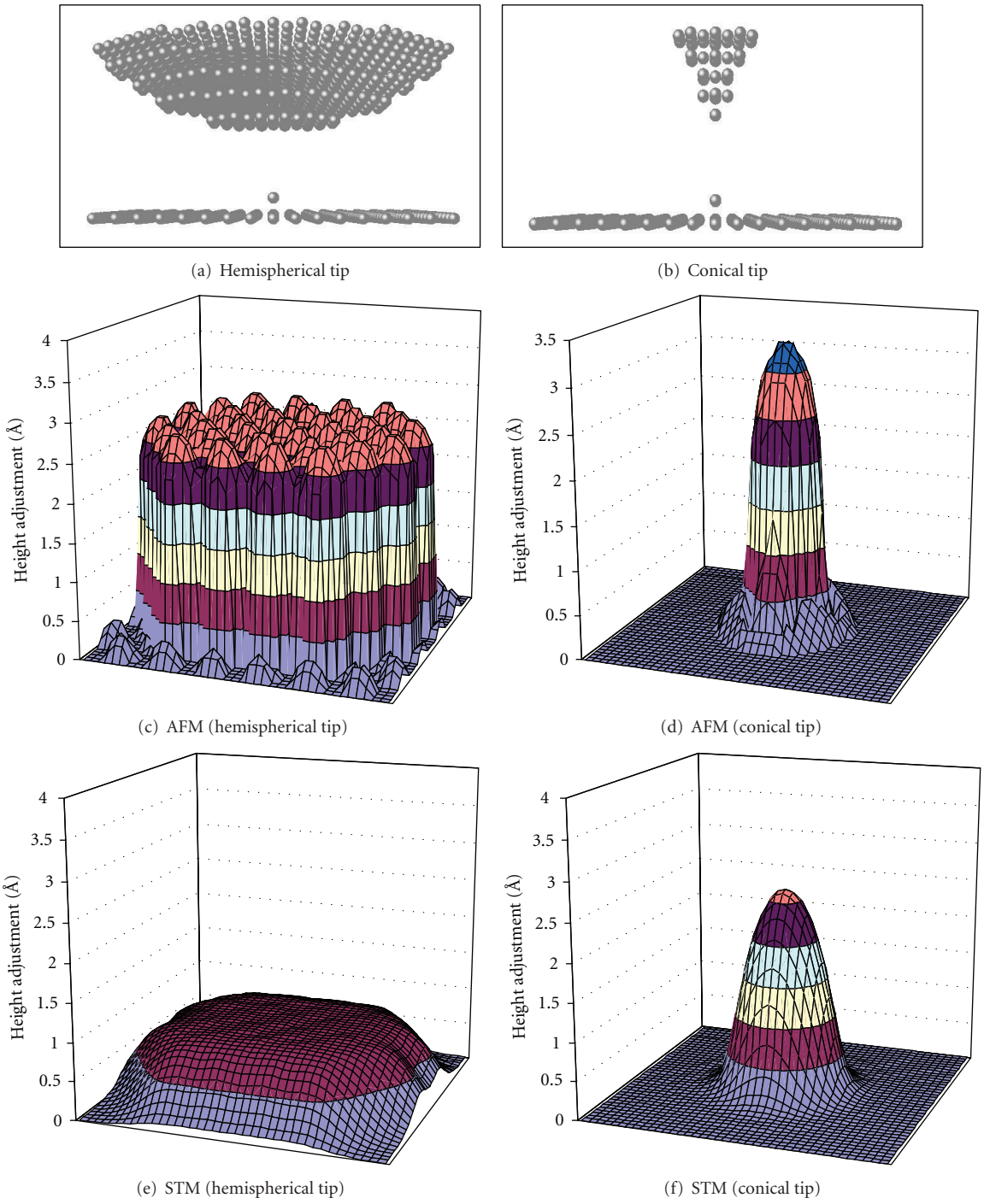

FIGURE 4: (a, b) Atomic structures of hemispherical and conical (aspect ratio = 1) 110-oriented W tips (radius 3 nm, lowest 5 atomic layers shown) scanning over a raised atom on a flat plane. Interatomic distances are to scale (sample atomic spacing = 2.5 Å); for clarity, tip-sample separation is larger than used in calculations and atoms are shown smaller than their derived radii. (c, d) Topographical images produced by simulated imaging of sample atom and surface in AFM mode by hemispherical and conical tips (setpoint defined as point of maximum attractive force). (e, f) Topographical images produced by simulated imaging of sample atom and surface in constant-current STM mode (same setpoint) by hemispherical and conical tips. Scanned area: 20×20 Å^2.

3. Results

3.1. Effect of Tip Size on Electric Field. The electric field F at the surface of a charged sphere of radius r at voltage V is given by the relation $F = V/r$. For a hemispherical tip at the end of a long shank, the relation is modified to $F = V/kr$ [8]. Lucier et al. [11] correlated the radii of W STM tips (measured using scanning electron microscope images) with the best imaging voltage and estimated a value of k of 3.3–3.4 for annealed tips with radii of 20–40 nm. Evaporation

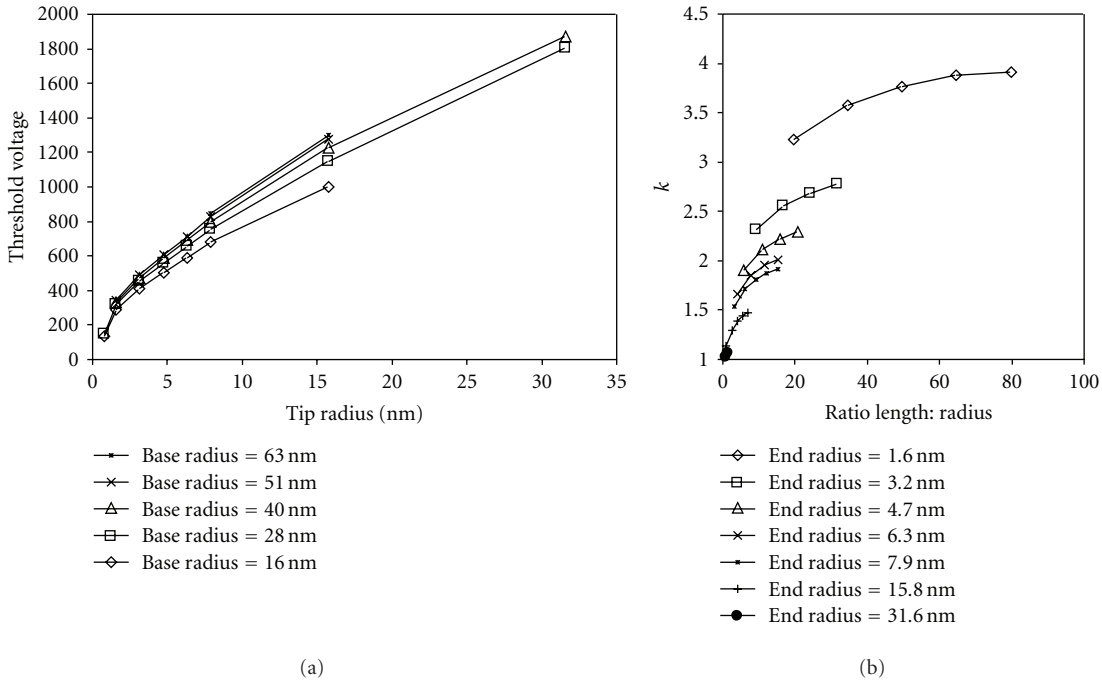

FIGURE 5: (a) Values of field evaporation threshold voltage for $W(110)$ tips consisting of a hemisphere on top of a conical shank for different shank and hemisphere sizes (b) effective values of field reduction factor κ as a function of the ratio of tip length to end radius. Cone aspect ratio = 1 (opening angle 51.2°).

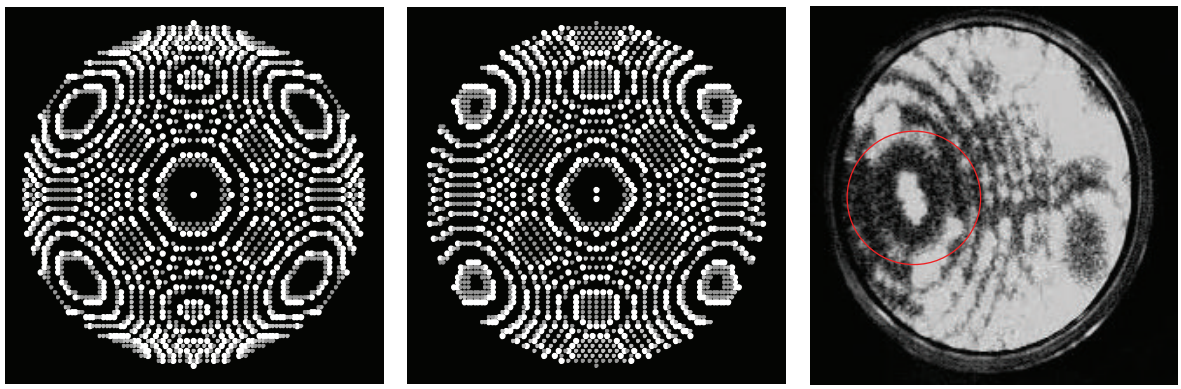

FIGURE 6: (a, b) Schematic FIM images of 110-oriented hemispherical W tip (radius 8 nm) subjected to field evaporation (image-force model without polarization component) at 77 K, single-atom and double tip; (c) experimental image of polycrystalline W tip (apex circled) imaged at 77 K, 8.0 kV.

and imaging took place from 2.4–6.2 kV. This is consistent with our experiments and other results from the literature—in general, where field evaporation is possible, it is carried out in the regime 10^3–10^4 V with sharper tips requiring lower voltages.

Figure 5(a) shows the applied voltage required for field evaporation (based on the value at which the activation energy equals zero under the image-force model) of conical $W(110)$ tips with a hemispherical cap under the model. The threshold voltage rises linearly with increasing end radius as expected (except for very small tips), and increases with the shank size. The effective value of k increases nonlinearly with the ratio of tip length to end radius (Figure 5(b)). For larger tips comparable to those examined by Lucier et al., the threshold voltage is at the lower end of the expected range and can be expected to rise for tips with larger radii or longer shanks (modelling of larger structures than those used to generate the data in Figure 5 is very time-consuming and was therefore not carried out).

Notably, although the size of the shank strongly affects the strength of the electric field around the tip, the field distribution near the apex is found to be very similar regardless of whether or not a long shank is present. Field evaporation therefore tends to remove the same atoms from the apex,

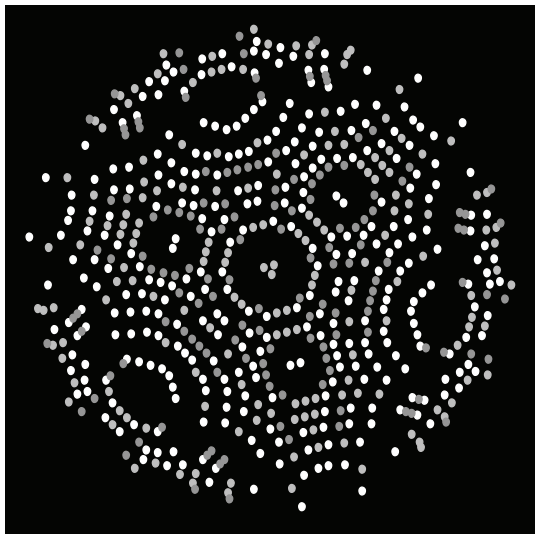

Figure 7: Schematic FIM image of 111-oriented hemispherical W tip (radius 13 nm) subjected to field evaporation at 77 K (image-force model without polarization component).

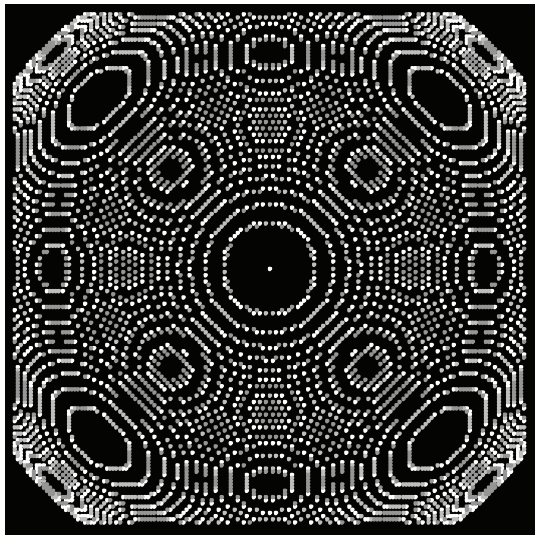

Figure 8: Schematic FIM image of 100-oriented hemispherical Pt tip (radius 16 nm) subjected to field evaporation at 77 K (image-force model without polarization component).

giving rise to the same configurations. Hence, the results presented below for the shapes of field-evaporated tips were derived from hemispherical tips without a large shank.

3.2. Evaporated Tip Structures for Different Materials. Figures 6–8 show schematic FIM images for three different types of tip subjected to field evaporation. Structures similar to those seen in the literature [1–3, 12–16] and our own experiments (Figure 6(c)–compare Figure 6(b)) are found, including faceting along close-packed crystal directions. SATs where the apex atom lies atop a flat terrace can be formed from $W(110)$ (Figure 6(a)) and Pt(100) (Figure 7), again as seen experimentally (Figure 3(c)). A symmetrical single-atom apex cannot be formed on $W(111)$—the sharpest symmetrical configuration is a trimer (Figure 8). If the tip is modelled in its entirety rather than using 3-fold symmetry, the atoms of the trimer can be removed one by one to produce an asymmetrical single-atom apex [14]. This again mirrors experimental results in the literature—a pyramidal apex consisting of a single atom atop the trimer can be formed by, for example, chemically etching the tip at high voltage [15] or depositing atoms from the gas phase [16], but not by field evaporation. This correspondence with well-documented experimental results confirms the validity of the model.

Simulations of the effect on STM and AFM resolution of using field-sharpened tips compared to their preevaporated forms are presented as supplementary material.

4. Conclusions

Field evaporation of atoms in the field ion microscope is simulated using an iterative finite difference method that builds on the work of Vurpillot et al. [6]. Our model differs from other work on simulation of FIM and atom probe experiments [4–6] due to its focus on field evaporation and changes in tip structure rather than on the trajectories of emitted ions. Mathematical models of field evaporation taken from the literature are compared, and it is found that the time-dependent kinetic models used all produce similar results which match experimental observations more closely than the simpler method used by Vurpillot et al. The field-evaporated endforms of tips made from materials suitable for SPM are modelled, with results in reasonable agreement with those seen experimentally in our own work and in the literature. The effect of field-induced tip sharpening on tip convolution in scanning probe microscopy is also simulated.

The simulation methods developed in this work are expected to be very useful in future STM/AFM experiments. In addition to aiding in the production of single-atom tips for improved resolution, it is hoped that improved understanding of the structure of such tips will aid the measurement and understanding of surface forces at an atomic level. If the surface atomic structure is determined by STM and the tip structure by FIM, then simulations of the interatomic forces can be refined via comparison with simultaneously gathered AFM data. In this way, more accurate mathematical models of surface forces may be produced.

Acknowledgments

The support of EU FP7 (Contract no. 214250) and Science Foundation Ireland (Grant no. 06/IN.1/I106) are gratefully acknowledged.

References

[1] Y. Kuk and P. J. Silverman, "Role of tip structure in scanning tunneling microscopy," *Applied Physics Letters*, vol. 48, no. 23, pp. 1597–1599, 1986.

[2] A. Fian and M. Leisch, "Study on tip-substrate interactions by STM and APFIM," *Ultramicroscopy*, vol. 95, pp. 189–197, 2003.

[3] T. An, T. Eguchi, K. Akiyama, and Y. Hasegawa, "Atomically-resolved imaging by frequency-modulation atomic force microscopy using a quartz length-extension resonator," *Applied Physics Letters*, vol. 87, no. 13, Article ID 133114, pp. 1–3, 2005.

[4] B. P. Geiser, D. J. Larson, S. S. A. Gerstl et al., "A system for simulation of tip evolution under field evaporation," *Microscopy and Microanalysis*, vol. 15, supplement 2, pp. 302–303, 2009.

[5] E. A. Marquis, B. P. Geiser, T. J. Prosa, and D. J. Larson, "Evolution of tip shape during field evaporation of complex multilayer structures," *Journal of Microscopy*, vol. 241, no. 3, pp. 225–233, 2011.

[6] F. Vurpillot, A. Bostel, and D. Blavette, "A new approach to the interpretation of atom probe field-ion microscopy images," *Ultramicroscopy*, vol. 89, no. 1–3, pp. 137–144, 2001.

[7] R. G. Forbes, "Field evaporation theory: a review of basic ideas," *Applied Surface Science*, vol. 87-88, pp. 1–11, 1995.

[8] M. K. Miller, A. Cerezo, M. G. Hetherington, and G. D. W. Smith, *Atom Probe Field Ion Microscopy*, Oxford Science Publications, 1996.

[9] H. J. Kreuzer and K. Nath, "Field evaporation," *Surface Science*, vol. 183, no. 3, pp. 591–608, 1987.

[10] D. N. J. White, "A computationally efficient alternative to the Buckingham potential for molecular mechanics calculations," *Journal of Computer-Aided Molecular Design*, vol. 11, no. 5, pp. 517–521, 1997.

[11] A. S. Lucier, H. Mortensen, Y. Sun, and P. Grütter, "Determination of the atomic structure of scanning probe microscopy tungsten tips by field ion microscopy," *Physical Review B*, vol. 72, no. 23, Article ID 235420, pp. 1–9, 2005.

[12] G. Cross, A. Schirmeisen, A. Stalder, P. Grütter, M. Tschudy, and U. Dürig, "Adhesion interaction between atomically defined tip and sample," *Physical Review Letters*, vol. 80, no. 21, pp. 4685–4688, 1998.

[13] T. V. de Bocarmé, T. D. Chau, and N. Kruse, "Imaging and probing catalytic surface reactions on the nanoscale: Field Ion Microscopy and atom-probe studies of O_2–H_2/Rh and NO–H_2/Pt," *Topics in Catalysis*, vol. 39, pp. 111–120, 2006.

[14] K. Motai, T. Hashizume, H. Lu, D. Jeon, T. Sakurai, and H. W. Pickering, "STM of the Cu(111)1×1 surface and its exposure to chlorine and sulfur," *Applied Surface Science*, vol. 67, no. 1–4, pp. 246–251, 1993.

[15] F. Rahman, J. Onoda, K. Imaizumi, and S. Mizuno, "Field-assisted oxygen etching for sharp field-emission tip," *Surface Science*, vol. 602, no. 12, pp. 2128–2134, 2008.

[16] H. W. Fink, "Mono-atomic tips for scanning tunneling microscopy," *IBM Journal of Research and Development*, vol. 30, p. 460, 1986.